On the Impact of Low-Rank Interference on the Post-Equalizer SINR in LTE

Fabian Monsees, Carsten Bockelmann, Mark Petermann, Armin Dekorsy, and Stefan Brueck

***Abstract*—The standardization of the fourth generation of mobile communication systems was mainly driven by the demands for higher data-rates and improved Quality of Service. To reach these goals interference coordination has been identified as a promising research field for better exploitation of the time and frequency resources. This paradigm shift from interference avoidance to interference coordination is also reflected in the ongoing enhancement of the 4th generation of mobile communication systems such as 3GPP Long Term Evolution. In this context, numerous investigations have focused on the allocation of precoding matrices that are part of the link adaptation process by some form of base station (eNB) coordination.**

Within this work we develop a non-centralized interference coordination scheme by noticing that the re-allocation of a precoding matrix can lead to an uncontrolled change of the interference level at users located in neighboring cells, especially at the edge. To this end, we provide a fully closed form mathematical framework describing these changes. Based on this, we derive a simple metric that improves the precoding matrix selection process in the User Equipment with the result that interference changes can be reduced without having any standard impact. This novel scheme can also be seen as an extension to previous inter-cell interference coordination schemes without the need of base-station cooperation.

***Index Terms*—Long Term Evolution, Inter-Cell Interference, Low-Rank Precoding, Bivariate Chi-Squared density, MIMO, Spatial Multiplexing**

I. Introduction

The application of multiple antennas at both the transmitter and the receiver allows for transmission of several data-streams at the same time. This space-time modulation scheme is known as spatial multiplexing and is applied to reach the performance gains promised by the application of the Multiple-Input Multiple-Output (MIMO) technique [1]. To perfectly match the data-streams to the underlying MIMO channel, precoding at the transmitter is necessary [2], e.g., via precoding matrices. One major drawback here is that optimal precoding with highest performance gains can only be achieved with full Channel State Information (CSI) at the transmitter, which requires a reliable and fast feedback channel in order to convey the estimated CSI from the receiver back to the transmitter. A reduction of feedback and complexity can be gained by pre-defining a limited set of precoding matrices where the receiver simply signals the index of its optimal precoding matrix back to the transmitter.

This technique is known as finite codebook matrix precoding [3] and is one possible space-time modulation scheme used in 3GPP Long Term Evolution to transmit the data streams from the evolved NodeB (eNB) to the User Equipment (UE). Furthermore, LTE is a cell based system where downlink transmissions within each cell are orthogonal such that intra-cell interference is avoided totally [4]. However, LTE implements a frequency reuse factor of one between cells, which makes inter-cell interference a performance limiting factor since cell edge users experience transmissions from the neighboring cells as inter-cell interference [5] [6].

A crucial point in this context is the allocation of a particular precoding matrix which determines the beamforming of the transmit antennas at the eNB. Especially, cell edge users see inter-cell interference that is dependent on the currently allocated precoding matrices at neighboring eNBs. This dependency of inter-cell interference and precoding matrix gives the motivation to consider the allocation of precoding matrices from an inter-cell interference coordination point of view. Previous research in this field has shown how the precoding matrix selection process can be optimized to mitigate inter-cell interference [7]. This goal can either be achieved by coordinating transmissions among neighboring eNBs [8], or by performing coordinated scheduling between serving eNBs [9][10]. The main focus thereby is either to cooperatively select precoding matrices that minimize inter-cell interference, or to avoid inter-cell interference by performing cooperative scheduling such that cell edge users from different cells are not scheduled on the same physical resource. These techniques are summarized as Coordinated Multi Point Transmission (CoMP), where eNBs cooperate in order to coordinate inter-cell interference [11].

All these investigations of inter-cell interference coordination have mainly focused on avoiding or minimizing the inter-cell interference level when a certain precoding matrix is applied. This work addresses the interference level directly before and after the re-allocation of a precoding matrix. In particular, we investigate the change of the interference level caused at a mobile when precoding matrices are re-allocated at neighboring base-stations. We show that especially in cases where the number of data-streams is lower than the number of transmit antennas, the re-allocation of a precoding matrix leads to a sudden and yet uncontrolled change in the interference and Signal to Interference plus Noise Ratio (SINR) level at UEs located in neighboring cells. This paper extents our investigations made in [12] where we derived the statistical description of the inter-cell interference and SINR level at a mobile that is exposed to inter-cell interference.

At first, we will evaluate a mathematical framework for inter-cell interference and SINR changes in the downlink at UEs

F. Monsees, C. Bockelmann, M. Petermann and A. Dekorsy are with the Institute for Telecommunications and High-Frequency Techniques / Department of Communications Engineering, University of Bremen, Germany, Email:{monsees, bockelmann, petermann, dekorsy}@ant.uni-bremen.de

S. Brueck is with Qualcomm CDMA Technologies, Nuremberg, Germany, Email: sbrueck@qti.qualcomm.com

that are exposed to inter-cell interference. The well studied dependency of precoding matrix and interference level is thereby extended by a fully closed form formulation of the probability density function (pdf) describing the change in the interference level caused by the re-allocation of a precoding matrix. Beyond that, we show that the correlation, which connects the interference levels before and after re-allocation, can be described by a simple expression involving only the two precoding matrices applied for the re-allocation. Based on the correlation, we obtain a simple metric that reflects the height of the change in the interference levels. Moreover, we utilize this metric to derive a novel and easily implementable UE specific precoding matrix selection strategy that augments currently applied inter-cell interference coordination schemes by focusing on jointly enhancing the SINR in a cell while reducing interference changes in neighboring cells. This consideration augments the existing inter-cell interference coordination techniques by avoiding sudden changes in the inter-cell interference and, consequently, in the SINR. Additionally our scheme can be implemented without the need of a base station cooperation and without having any standard impact.

The remainder of this paper is structured as follows. In Section II we introduce our LTE compliant system model incorporating K interfering eNBs. The pdf of the change in the inter-cell interference caused by the re-allocation of the precoding matrix in a single interferer scenario is derived as the ratio distribution of a bi-variate chi-squared pdf in Section III. Section IV investigates the change in the SINR caused by the change of the interference level. The resulting pdfs are presented in Section V. The novel precoding matrix selection strategy is introduced in Section VI, where we introduce a new weighting rule that aims at mitigation of SINR changes in neighboring cells while simultaneously enhancing the SINR in the current cell. The performance analysis of this rule is analyzed in Section VI-A. Finally conclusions are drawn and an outlook is given in Section VII.

1) Notation: We apply the following notation in the remainder of this work. Matrices are denoted by capital bold characters $\mathbf{A}$. Small bold characters, $\mathbf{a}$, denote a column vector, and $\mathbf{a}_{(i)}$ stands for the ith column vector of the matrix $\mathbf{A}$ and $\mathbf{a}^{(i)}$ denotes the ith row vector. $[\mathbf{A}]_{i,i}$ is the ith diagonal element of the matrix $\mathbf{A}$. The expectation of a process is expressed as $\mathrm{E}(\cdot)$ and $\mathrm{Tr}(\cdot)$ denotes the trace of a matrix. We express the Gamma function as $\Gamma(\cdot)$ with $\Gamma(n) = (n-1)!$. The $\mathrm{stdev}(\cdot)$ operation calculates the standard deviation, $\mathrm{mean}(\cdot)$ the mean of a process. $\mathrm{cov}(\cdot;\cdot)$ denotes the covariance between two processes. The inner vector product is expressed as $\langle\cdot;\cdot\rangle$. We express a complex circular Gaussian distribution with mean μ and variance σ^2 as $\mathcal{N}_C\left(\mu,\sigma^2\right)$. Analogously, a chi-squared distribution with N degrees of freedom is expressed as χ^2_N. $\mathbf{I}_{L_0}$ denotes the identity matrix of dimension $L_0 \times L_0$.

II. System Model

Within this work we assume a setup involving $K+1$ different cells where the serving eNB per cell is denoted as eNB_k with $k \in [0...K]$. To simplify the description we assume UE_0 that is served by eNB_0 and is interfered by eNB_k transmitting signals to UE_k. Transmissions within a cell are orthogonal and, hence, we focus on inter-cell interference only. Fig. 1 shows an example of the general setup involving

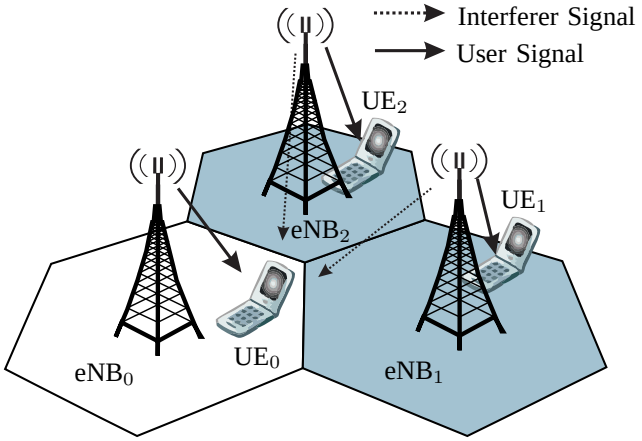

Fig. 1. Exemplary setup where UE_0 is served by eNB_0 in its cell. The transmissions from eNB_1 and eNB_2 to UE_1 and UE_2, respectively, are received as interference power

$K+1=3$ eNBs. UE_0 is served by eNB_0 and is located at the edge of its cell, surrounded by $K=2$ interfering eNBs that are serving the UEs in their cells. These transmissions are experienced as interference at UE_0.

Generally, all $K+1$ eNBs are assumed to communicate to their UEs over a $T_k \times R_k$ MIMO channel where T_k denotes the number of transmit antennas at eNB_k and R_k denotes the number of receive antennas at UE_k, respectively. All eNBs transmit $L_k \leq \min(T_k, R_k)$ independent data-streams, which are called layers in the LTE context, simultaneously to their UEs. These layers are linearly precoded by a $T_k \times L_k$ precoding matrix denoted as $\mathbf{B}_k \in \mathbf{\Gamma} = \{\mathbf{\Gamma}_1, ..., \mathbf{\Gamma}_C\}$. The codebook $\mathbf{\Gamma}$ is predefined, of finite cardinality C and stored at each eNB. For our investigation we assume the codebook as specified in the LTE standard [5]. In case of $L_k = T_k$ the precoding matrices can be written as $\mathbf{B}_k = 1/\sqrt{L_k}\mathbf{U}$ with $\mathbf{U}$ being a unitary matrix. If $L_k \leq T_k$, the transmission is termed low-rank and the precoding matrices are constructed by simply removing $T_k - L_k$ column vectors in $\mathbf{B}_k$. This procedure is described in the corresponding LTE standardization bodies [5]. In the sequel we consider the estimated signal vector $\hat{\mathbf{x}}$ at the output of the equalizer at UE_0 in the presence of K interfering eNBs by

$$\hat{\mathbf{x}} = \mathbf{G}\mathbf{H}_0\mathbf{B}_0\mathbf{x}_0 + \mathbf{G}\sum_{k=1}^{K}\tilde{\mathbf{H}}_k\mathbf{B}_k\mathbf{x}_k + \mathbf{G}\mathbf{w}. \quad (1)$$

For channel equalization, we assume a linear equalizer denoted as $\mathbf{G} \in \mathbb{C}^{L_0 \times R_0}$ at UE_0. The downlink channel from eNB_k to UE_k is modeled as $\mathbf{H}_k \sim \mathcal{N}_C(0,1) \in \mathbb{C}^{R_k \times T_k}$ and the interferer channels from the interfering eNBs to UE_0 are modeled as $\tilde{\mathbf{H}}_k \sim \mathcal{N}_C(0,1) \in \mathbb{C}^{R_0 \times T_k}$ [13]. The transmit signal vector $\mathbf{x}_k = [x_{k,1}, ..., x_{k,L_k}]^T \in \mathbb{C}^{L_k}$ is assumed to obey a zero mean uncorrelated process with covariance matrix $\mathrm{E}\left(\mathbf{x}_k\mathbf{x}_k^H\right) = \sigma_k^2\mathbf{I}_{L_k}$, where σ_k^2 denotes the signal power transmitted by eNB_k. The complex baseband noise vector $\mathbf{w}$ with covariance matrix $\sigma_w^2\mathbf{I}_{R_0}$ is modeled as $\mathbf{w} \sim \mathcal{N}_C(0, \sigma_w^2) \in \mathbb{C}^{R_0}$.

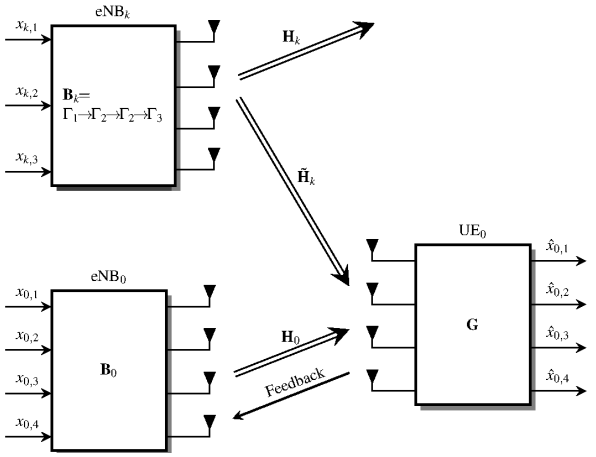

Fig. 2. Single low-rank interferer scenario. eNB$_k$ changes its low-rank precoding matrix from $\mathbf{B}_k(n)$ to $\mathbf{B}_k(n+1)$

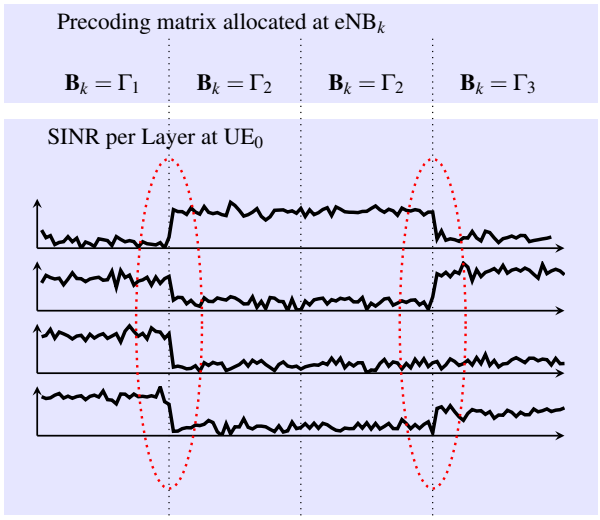

Fig. 3. Illustration of SINR change per layer caused by a precoder changes at a low-rank interfering eNB

A. Problem Statement

Subsequently, we pose the methodology of low-rank precoding and the problems caused. Considering (1) it is obvious that the inter-cell interference is determined by $\mathbf{B}_k$. Therefore, if eNB$_k$ reallocates its precoding matrix $\mathbf{B}_k$ for UE$_k$ the inter-cell interference changes, i.e., the SINR at UE$_0$ changes. As shown later, the change of inter-cell interference is for low-rank precoding only, thus we focus on low-rank precoding, i.e., $L_k < \min(T_k, R_k)$, $\forall k$. A more detailed insight into the main problem that we address is given on Fig. 2. Here UE$_0$ is assumed to be located at the edge of its cell and is served by eNB$_0$ over the channel $\mathbf{H}_0$. eNB$_k$ serves UE$_k$ in its cell over the channel $\mathbf{H}_k$. The transmission takes place on the same physical resources as UE$_0$ is served and, consequently, UE$_0$ experiences these transmission as inter-cell interference over the interferer channel $\tilde{\mathbf{H}}_k$. eNB$_k$ is now assumed to communicate to UE$_k$ with low-rank, here $L_k = 3$ layer over $T_k = R_k = 4$ antennas. In this example, we assume that eNB$_k$ reallocates the precoding matrix for UE$_k$ in the order $\mathbf{B}_k = \mathbf{\Gamma}_1 \rightarrow \mathbf{\Gamma}_2 \rightarrow \mathbf{\Gamma}_2 \rightarrow \mathbf{\Gamma}_3$ (Note that this reallocation is arbitrary and is solely meant for illustrating the problem). As a consequence of this re-allocation of low-rank precoding matrices, UE$_0$ experiences sudden changes in the interference power, leading to a sudden change in its SINR as shown in an illustrative way on Fig. 3. It is shown that the SINR level on the received layers changes suddenly if the precoding matrix is re-allocated at eNB$_k$. The dotted ellipses emphasize the particular SINR changes experienced at UE$_0$.

To derive the analytical framework for the description of the inter-cell interference level change and the SINR level change at UE$_0$ we consider the two time instances where eNB$_k$ $k \in [1...K]$ reallocates a precoding matrix to UE$_k$. We denote the time instance before re-allocation as n and after re-allocation as $n+1$. The precoding matrices applied at these time instances are denoted as $\mathbf{B}_k(n) \in \mathbf{\Gamma}$ and $\mathbf{B}_k(n+1) \in \mathbf{\Gamma}$, respectively.

We further define the post-equalizer SINR on the ith layer at UE$_0$ at the two time instances n and $n+1$ as

$$\gamma_i(n) = \frac{S_i}{I_i + \psi_i(n) + w_i} \; i = 1...L_0, \tag{2a}$$

$$\gamma_i(n+1) = \frac{S_i}{I_i + \psi_i(n+1) + w_i} \; i = 1...L_0, \tag{2b}$$

where S_i denotes the signal power, I_i the inter-layer interference after equalization, w_i denotes the mean noise power, $\psi_i(n)$ and $\psi_i(n+1)$ denote the inter-cell interference caused by interfering eNBs on the ith layer at UE$_0$ before and after re-allocation of precoding matrices. We assume that all quantities in (2a) and (2b) except $\psi_i(n)$ and $\psi_i(n+1)$ are the same in time instance n and $n+1$. We further have

$$w_i = \underset{\mathbf{w}}{\mathrm{E}}\left(\|\mathbf{g}^{(i)}\mathbf{w}\|_2^2\right) = \|\mathbf{g}^{(i)}\|_2^2 \sigma_w^2 \tag{3}$$

as the mean of the noise power at the equalizer output at UE$_0$.

Remark 1: It should be noted that the change in the inter-cell interference at UE$_0$ can also be caused by a scheduling decision at eNB$_k$. Instead of reallocating the precoding matrix for UE$_k$ the serving eNB (eNB$_k$) can also schedule a different UE (UE$_{k'}$) with another precoding matrix ($\mathbf{B}_{k'}$) on the physical resource where UE$_0$ is scheduled.

III. The Inter-Cell Interference Change

The previous section motivated that sudden changes in the inter-cell interference result in changes in the SINR level. In this section we give a statistical description of the change in the interference level which is extended further to involve the change in the SINR level. First, we consider a single interferer scenario, while, the results for arbitrary numbers of interferer are evaluated later on. With (1) we introduce the post-equalizer inter-cell interference vector for the time instance n as

$$\mathbf{v} = \mathbf{G}\tilde{\mathbf{H}}_k\mathbf{B}_k(n)\,\mathbf{x}_k \;\; 1 \le k \le K. \tag{4}$$

The post-equalizer interference covariance matrix for the nth time instance is thus given by

$$\mathbf{R}(n) = \underset{\mathbf{x}_k}{\mathrm{E}}\left(\mathbf{v}\mathbf{v}^H\right) = \sigma_k^2\mathbf{G}\tilde{\mathbf{H}}_k\mathbf{B}_k(n)\,\mathbf{B}_k^H(n)\,\tilde{\mathbf{H}}_k^H\mathbf{G}^H, \tag{5}$$

and, the diagonal elements $[\mathbf{R}(n)]_{v,v}$ of $\mathbf{R}(n)$ are the inter-cell interference at the equalizer outputs at UE_0. Under the condition that the equalizer matrix is independent of the precoding matrix applied at the interfering eNB, i.e., $\mathbf{G} \neq f(\mathbf{B}_k)$, we showed in [12] that $[\mathbf{R}(n)]_{v,v}$ obey for full-rank and for low-rank precoding to a scaled chi-squared distribution with $2L_k$ degrees of freedom, which can be written as

$$[\mathbf{R}(n)]_{v,v} = \psi_i(n) = \|\mathbf{g}^{(v)}\|_2^2 \frac{\sigma_k^2}{2L_k} u(n), \qquad (6)$$
$$u(n) \sim \chi^2_{2L_k}.$$

Here, $u(n)$ is a chi-squared distributed random variable.
In case of full-rank precoding we have $\mathbf{B}_k = 1/\sqrt{L_k}\mathbf{U}$ and $\mathbf{U}\mathbf{U}^H = \mathbf{I}$ and with (5) we obtain

$$\mathbf{R}(n) = \frac{\sigma_k^2}{L_k} \mathbf{G}\tilde{\mathbf{H}}_k \tilde{\mathbf{H}}_k^H \mathbf{G}^H, \qquad (7)$$

which is independent of $\mathbf{B}_k \in \mathbf{\Gamma}$.
Therefore, our analysis focuses on the impact of low-rank precoding on the inter-cell interference and on the SINR. We define the change in the inter-cell interference as

$$z_{i,\text{dB}} = 10\log_{10}(z_i) \text{ with } z_i = \frac{\psi_i(n)}{\psi_i(n+1)},\ i = 1...L_k. \quad (8)$$

With (8) we first evaluate z_i and afterwards the transformation into log-domain. In our model we assume that only $\mathbf{B}_k$ changes from the time instance n to $n+1$. The channel matrix $\tilde{\mathbf{H}}_k$ is of minor importance. It reflects the channel from the interfering eNB to UE_0 only for the time instance where the precoding matrix in the interfering cell in re-allocated. This justifies the assumption of a Gaussian matrix. Moreover, the change in the inter-cell interference is a short term effect which is not affected by long-term fading. We show in Appendix A, that the definition of the interference covariance matrix given in (5) allows to express z_i as the quotient of the diagonal elements $[\mathbf{R}(n)]_{v,v}$ and $[\mathbf{R}(n+1)]_{v,v}$. Thus we obtain with (6), (8) and Appendix A

$$z_i = \frac{\psi_i(n)}{\psi_i(n+1)} = \frac{\sum_{l=1}^{L_k}\left(\tilde{\mathbf{h}}_k^{(i)}\mathbf{b}_{k,(l)}(n)\right)^2}{\sum_{l=1}^{L_k}\left(\tilde{\mathbf{h}}_k^{(i)}\mathbf{b}_{k,(l)}(n+1)\right)^2} := \frac{\sum_{l=1}^{L_k} x_l}{\sum_{l=1}^{L_k} y_l}$$
$$\text{where } x_l, y_l \sim \chi_2^2. \qquad (9)$$

Most interestingly, (9) shows no dependency on the interferer-power σ_k^2 itself and, consequently, the change in the inter-cell interference is independent of the interferer power. We show in Appendix D that the correlation of element x_i with y_j in (9) can be expressed as

$$\rho_{x_i,y_j} = \langle \mathbf{b}_{k,(i)}(n), \mathbf{b}_{k,(j)}(n+1)\rangle^2 L_k^2 \ \forall i,j \in 1...L_k. \quad (10)$$

Thus we define the following $L_k \times L_k$ matrix that expresses the correlation between all elements of numerator and denominator of (9)

$$\mathbf{\Phi}_{x,y} = \begin{bmatrix} \rho_{x_1,y_1} & \rho_{x_1,y_2} & \cdots & \rho_{x_1,y_{L_k}} \\ \rho_{x_2,y_1} & \rho_{x_2,y_2} & \cdots & \rho_{x_2,y_{L_k}} \\ \vdots & \vdots & \vdots & \vdots \\ \rho_{x_{L_k},y_1} & \rho_{x_{L_k},y_2} & \cdots & \rho_{x_{L_k},y_{L_k}} \end{bmatrix}. \qquad (11)$$

Note that the correlation between all random variables in numerator and denominator in (9) are zero, i.e., $\rho_{x_i,x_j} = \rho_{y_i,y_j} = 0,\ i \neq j$.

A. PDF for Single Interfering eNB

Considering the definition given in (9), we see that the dependency on the layer index i at UE_0 is only due to the ith column vector $\tilde{\mathbf{h}}_k^{(i)}$ of the interferer channel matrix $\tilde{\mathbf{H}}_k$. Note that the statistical properties of z are thus independent of the layer index considered. With (11) we see that the pdf of (9) is the ratio-density r of a multivariate chi-squared density

$$f_z(z) = r\left(f_{\chi^2}(x_1,...,x_{L_k},y_1,...,y_{L_k},\mathbf{\Phi}_{x,y})\right). \qquad (12)$$

Eq. (12) clearly shows that the pdf of z has to be expressed by a multivariate chi-squared distribution with at least L_k^2 parameters describing the correlation between the marginals. Since closed form pdfs for multivariate chi-squared pdfs exist in literature up to the tri-variate case [14], we introduce the following simplification where we utilize a bi-variate chi-squared distribution [15] to derive the pdf of z. We thereby interpret numerator and denominator of (9) as a chi-squared distribution with each $2L_k$ degrees of freedom, as derived in [12]. This interpretation allows to utilize a single parameter to describe the correlation between numerator and denominator which we interpret as the marginals of a bi-variate chi squared density. This method will provide the exact pdf for z in case of single layer interfering eNBs. If the interferer rank increases, an approximation for the true pdf of z can be obtained though by choosing the degrees of freedom appropriately. With (9) the change in the inter-cell interference can now be written as

$$z_i = \frac{\sum_{l=1}^{L_k} x_l}{\sum_{l=1}^{L_k} y_l} = \frac{u(n)}{u(n+1)}, \quad u(n), u(n+1) \sim \chi^2_{2L_k}. \quad (13)$$

The derivation of the pdf $f_{z_i}(z_i)$ and its logarithmic transform $f_{z_i,\text{dB}}(z_{i,\text{dB}})$ can be found in Appendix B.

Here, the interference powers at the time instances n and at $n+1$ are interpreted as a single chi-squared distribution with $2L_k$ degrees of freedom. This allows a single correlation coefficient to describe the correlation between $u(n)$ and $u(n+1)$. As derived in Appendix D this single correlation coefficient can be calculated by

$$\rho_{u(n),u(n+1)} = \text{Tr}\left(\mathbf{B}_k^H(n+1)\mathbf{B}_k(n)\mathbf{B}_k^H(n)\mathbf{B}_k(n+1)\right)L_k. \qquad (14)$$

Consequently, we calculate the approximate pdf for z_i by solving

$$f_{z_i}(z_i) = r\left(f_{\chi^2}\left(u(n), u(n+1), \rho_{u(n),u(n+1)}\right)\right). \quad (15)$$

With the derivation in Appendix B the pdf of the change in the inter-cell interference is expressed by (16) and the transformation of (16) into log-scale is expressed by

$$f_{z_\text{dB}}(z_\text{dB}) = 10^{\frac{z_\text{dB}}{10}-1}\log(10) f_z\left(10^{\frac{z_\text{dB}}{10}}\right). \qquad (17)$$

Note that due to the approximation made in (13), the exact pdf for z_i is obtained for $L_k = 1$ layer systems. For $L_k > 1$, (16) yields an approximated pdf.

$$f_z(z) = \frac{1}{2^{2L_k}\sqrt{\pi}\Gamma(L_k)(1-\rho)^{L_k}} \sum_{n=0}^{\infty} \left[\frac{\sqrt{\rho}}{1-\rho}\right]^{2n} \frac{\Gamma\left(\frac{2n+1}{2}\right)\Gamma(2n+2L_k)\, z^{n+L_k-1}}{(2n)!\Gamma(n+L_k)} \left[\frac{2(1-\rho)}{1+z}\right]^{2n+2L_k} \tag{16}$$

Remark 2: In case of multiple interfering eNBs, where each interfering eNB changes its precoding matrix from the time instance n to $n+1$, it is easy to show that the correlation coefficient connecting the experienced interference powers at both time instances can be calculated by

$$\rho_{u(n),u(n+1),\mathrm{K}} = \frac{\sum_{k=1}^{K} \sigma_k^4 \rho_{u(n),u(n+1),k}}{\sum_{k=1}^{K} \sigma_k^4}. \tag{18}$$

The main point here is that each interfering eNB that changes a precoding matrix contributes to the overall correlation coefficient weighted by the squared transmit power of the individual eNB.

IV. The Change in the Post-Equalizer SINR

All results obtained in the previous section can be extended to derive the change of the SINR caused by the change in the inter-cell interference which, as shown, is due to the reallocation of the precoding matrix at an interfering eNB. We therefore use our definitions of the SINR (2a) and (2b) at the two time instances n and $n+1$. Analogous to to the change in the interference given in (9) we define the change in the SINR as

$$\begin{aligned}
\tilde{z}_i &= \frac{\gamma_{i,n}}{\gamma_{i,n+1}} = \frac{I_i + \psi_i(n) + n_i}{I_i + \psi_i(n+1) + n_i} \\
&= \frac{I_i + \|\mathbf{g}^{(i)}\|_2^2 \frac{\sigma_k^2}{2L_k} u(n) + n_i}{I_i + \|\mathbf{g}^{(i)}\|_2^2 \frac{\sigma_k^2}{2L_k} u(n+1) + n_i} \\
&= \frac{2L_k \frac{I_i+n_i}{\|\mathbf{g}^{(i)}\|_2^2\sigma_k^2} + u(n)}{2L_k \frac{I_i+n_i}{\|\mathbf{g}^{(i)}\|_2^2\sigma_k^2} + u(n+1)} \\
&= \frac{\xi_i + u(n)}{\xi_i + u(n+1)} \quad \text{with } u(n), u(n+1) \sim \chi^2_{2L_k}
\end{aligned} \tag{19}$$

Generally, the pdf of $\tilde{z}_i$ has to be parametrized analogous to (9) by L_k^2 correlation coefficients. We again apply the bivariate chi-square model and note that (19) can be found as the ratio distribution of two shifted correlated chi-square distributed random variables. The derivation of the pdf $f_{\tilde{z}_i}(\tilde{z}_i)$ and the transformation into dB scale, i.e., to $f_{\tilde{z}_{i,\mathrm{dB}}}(\tilde{z}_{i,\mathrm{dB}})$ can be found in Appendix C.

Remark 3: The definition

$$\xi_i = 2L_k \frac{I_i + n_i}{\|\mathbf{g}^{(i)}\|_2^2 \sigma_k^2} \tag{20}$$

shows that ξ_i denotes the ratio of inter-layer interference plus baseband noise to inter-cell interference and can be interpreted at the ratio of interfering effects from the serving cell to inter-cell interference coming from other cells. ξ_i is an abstract value that reflects the performance of the equalizer applied at the UE with respect to noise and interference suppression. The introduction of ξ_i allows us to summarize the performance of the receiver at the UE, which is not specified in the LTE standardization bodies. Furthermore, we assume that ξ_i does not change from the time instance n to $n+1$, which implies that the linear filter matrix $\mathbf{G}$ is independent of the realization of the inter-cell interference.

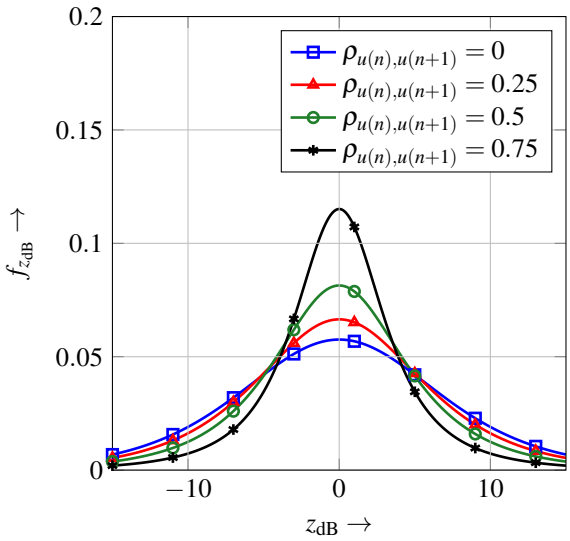

Fig. 4. PDFs for the change in the inter-cell interference for a single layer interfering eNB, parametrized by the correlation ρ.

V. Evaluation of Analytical Results

This section provides a graphical presentation of the pdf for the change in the inter-cell interference and of the resulting change in the SINR, parameterized by ξ_i. Figure 4 shows the evaluation of the closed form pdf (16) of the change in the inter-cell interference, z_{dB}, for different correlation coefficients for a single $L_1 = 1$ interfering eNB. It can be observed that the standard deviation of the density function decreases for high correlation coefficients. However, changes of up to ± 15 dB can still occur with a non-vanishing probability. Subsequently, the pdf is symmetric around 0 dB and the probability of a change to a higher or to a lower interference level is $1/2$. In any case, a UE experiencing a change in the interference level will request a change of its link adaptation by signaling the improved or decreased channel condition to its serving eNB. Even if the change in the interference level can also lead to better conditions for the UE considered, uncontrolled changes in the interference level will complicate scheduling decisions and increase the scheduling complexity. Moreover, an uncontrolled varying interference level will result in changes in the SINR that also have to be compensated by the link adaptation.

To show how the number of spatial layers affects the pdf of z_{dB}, Fig. 5 shows the approximated pdfs of z_{dB} for an interfering eNB transmitting $L_k = 3$ spatial layers leading to pdfs with a significantly decreased standard deviation compared to the single layer scenario. It was stated in [12] that the coefficient of variation for the inter-cell interference decreases with $\frac{1}{\sqrt{L_k}}$, this leads to narrower marginal densities $u(n)$ and

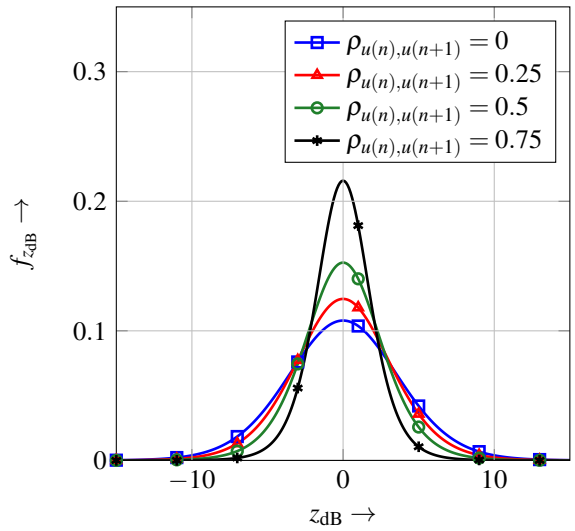

Fig. 5. Approximated pdfs for the chane in the inter-cell interference for an $L_k = 3$ layer interfering eNB, parametrized by the correlation coefficent ρ.

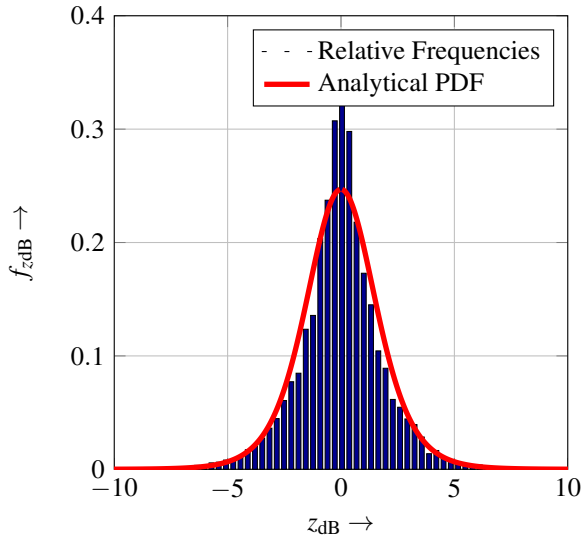

Fig. 6. Performance analysis of pdf approximation for a $L_k = 3$ layer interfering eNB switching between the precoding matrices $\Gamma_0 \rightarrow \Gamma_6$

$u(n+1)$ with decreased variances, which leads to a narrower pdf of z_{dB}. Again, a higher correlation coefficient leads to a pdf with lower standard deviation.

However, as already stated previously, the pdfs given in Fig. 5 approximate the true pdfs because the necessary correlation matrix $\mathbf{\Phi}_{x,y}$ is approximated by (14). To prove that this approximation is still feasible for our investigations, the following figure allows a comparison between the approximated pdf and relative frequencies obtained by Monte-Carlo simulation involving 10000 realizations for $\mathbf{H}_k$. Obviously Fig. 6 shows that our closed form pdf yields a good tail approximation for the true pdf. Henceforth, replacing the true correlation matrix that is necessary for the accurate pdf by a single value results in a slight approximation error. In this particular example the true correlation matrix reads

$$\mathbf{\Phi}_{x,y} = \begin{bmatrix} 0.0732 & 0.4268 & 0.4268 \\ 0.0732 & 0.4268 & 0.4268 \\ 0.4268 & 0.0732 & 0.0732 \end{bmatrix}. \quad (21)$$

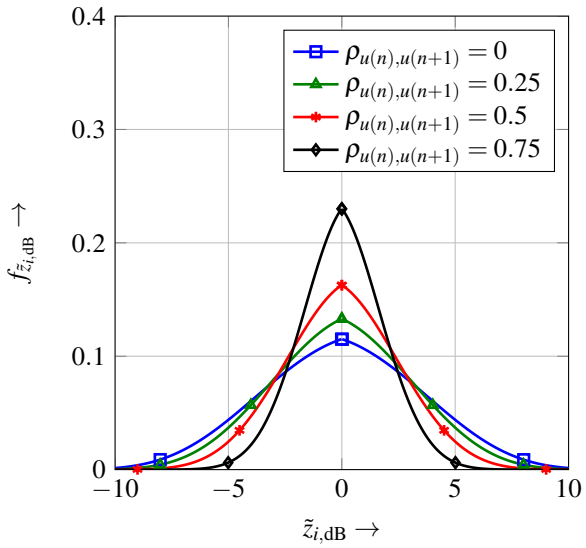

Fig. 7. PDFs of the change in the SINR caused by the re-allocation of the precoding matrix at an $L_k = 1$ layer interfering eNB $\xi_i = 0$ dB

According to the approximation given by (16) the single correlation coefficient between the interferer powers $u(n)$ and $u(n+1)$ is calculated as $\rho_{u(n),u(n+1)} = 0.8$ to obtain the approximated closed form pdf. Contrary to the pdf of z_{dB}, the closed form pdf (50) describing the SINR change $\tilde{z}_{i,\text{dB}}$ is parametrized by ξ_i which was introduced in (20). As stated previously, we utilize ξ_i as an abstract measure to summarize side effects such as the receiver performance and the inter-cell interference power. In the following a scenario with a single $L_1 = 1$ interfering eNB, which reallocates its precoding matrix and thereby causes a sudden change in the SINR at UE_0 is investigated. Fig. 7 shows the pdf of $\tilde{z}_{i,\text{dB}}$ at UE_0 parametrized by $\xi_i = 0$ dB. This could occur, e.g., if UE_0 is located close to the cell edge and thereby experiences a high inter-cell interference. The pdf is again symmetric around 0 dB and has a lower standard deviation if the correlation which is determined by the precoding matrices is increased. The impact of the change in the inter-cell interference on the SINR is decreased if ξ_i increases. For comparison Fig. 8 shows a setup with $\xi_i = 10$ dB. Obviously, the impact of the inter-cell interference is not as prominent as it is in the preceding example. Here, the pdfs of $\tilde{z}_{i,\text{dB}}$ have a decreased standard deviation. Again a higher correlation coefficient leads to a pdf with a lower standard deviation. The major key point concluding this section is that aiming at a high correlation while reallocating the precoding matrices results in a potentially lower change in the interference and SINR at UEs in neighboring cells.

VI. Reduction of uncontrolled changes in the SINR

The re-allocation of the precoding matrix was shown to cause a change in the inter-cell interference, leading to a change in the SINR especially at cell edge UEs. Our derivations have shown that this short term effect can be reduced if the correlation between two precoding matrices defined by (14) is kept at maximum whenever a precoding matrix is reallocated. Especially in LTE, UEs have the possibility

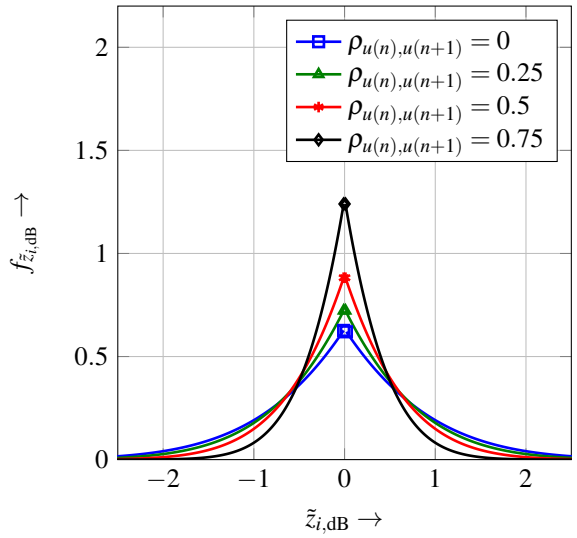

Fig. 8. PDFs of the change in the SINR caused by the re-allocation of the precoding matrix at an $L_k = 1$ layer interfering eNB $\xi_i = 10$ dB

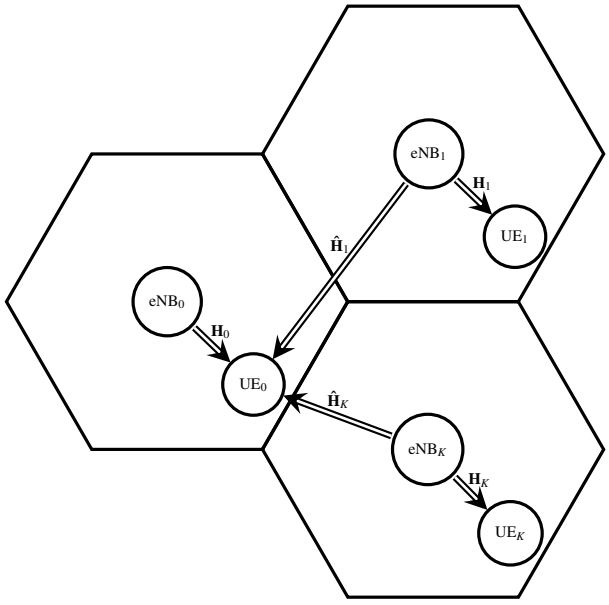

Fig. 9. Simulation setup, UE$_0$ is served by eNB$_0$ while K UEs in neighboring cells are served at the same frequency time resource.

to request a change of a precoding matrix at their serving eNBs for SINR maximization. Consequently, a reduction of changes in the SINR for the overall system can be obtained if each UE in a system tries to maximize correlation between precoding matrices. For a practical implementation, each UE has to find a trade-off between maximizing its individual SINR and minimizing SINR changes seen by other UEs. A practical implementation could involve the calculation of the following cost function at each UE.

$$\begin{aligned}&\mathbf{B}_k^{\star}(n+1) = \\ &\max (1-w) J_{\mathrm{SINR}}(\mathbf{B}_k(n+1)) + w J_{\mathrm{corr}}(\mathbf{B}_k(n+1), \mathbf{B}_k(n)) \\ &\text{s.t. } 0 \leq w \leq 1,\ \mathbf{B}_k(n+1) \in \mathbf{\Gamma}\end{aligned} \tag{22}$$

Here, the function

$$\begin{aligned}&J_{\mathrm{SINR}}(\mathbf{B}_k(n+1)) = \\ &\mathrm{Tr}\left(\mathbf{H}_k \mathbf{B}_k(n+1) \mathbf{B}_k^H(n+1) \mathbf{H}_k^H\right)\end{aligned} \tag{23}$$

aims at maximizing the squared singular values of $\mathbf{H}_k \mathbf{B}_k(n+1)$ and can be interpreted as maximizing the capacity of the resulting channel with precoding included. To maximize correlation in the interference level, we define

$$\begin{aligned}&J_{\mathrm{corr}}(\mathbf{B}_k(n+1), \mathbf{B}_k(n)) = \\ &\mathrm{Tr}\left(\mathbf{B}_k^H(n) \mathbf{B}_k(n+1) \mathbf{B}_k^H(n) \mathbf{B}_k(n+1)\right) L_k\end{aligned} \tag{24}$$

as the corresponding cost function for maximizing the correlation in the inter-cell interference experienced at cell edge UEs in neighboring cells if the serving eNB allocates $\mathbf{B}_k(n+1)$ while $\mathbf{B}_k(n)$ is allocated currently. To jointly optimize both cost functions, the weighting parameter $w \in [0...1]$ determines if a UE aims at maximizing its individual SINR $w = 0$, or if the UE aims at minimizing SINR changes in neighboring cells $w = 1$. In a practical setup a trade-off between both goals has to be found. However, this trade-off will result in an SINR loss at each UE that can be quantified by evaluating

$$\gamma_{\mathrm{loss},k} = 10 \log 10 \left(\frac{J_{\mathrm{SINR}}\left(\mathbf{B}_k^{\dagger}(n+1)\right)}{J_{\mathrm{SINR}}\left(\mathbf{B}_k^{\star}(n+1)\right)} \right), \tag{25}$$

where $\mathbf{B}_k^{\dagger}(n+1)$ is the index of the optimal precoding matrix in the context of SINR maximization, i.e., (22) with $w = 0$, and $\mathbf{B}_k^{\star}(i+1)$ is the the selected precoding matrix obtained by (22). We measure the performance of applying (22) by considering the standard deviation of the change in the SINR, i.e., stdev $(\tilde{z}_{i,\mathrm{dB}})$ at UE$_0$ and by the mean SINR loss defined as $\bar{\gamma}_k = \mathrm{E}(\gamma_{\mathrm{loss},k})$ experienced at UE$_k, k \in [1...K]$.

A. Setup

To assess the performance of the previously introduced precoding matrix selection rule, we consider the scenario depicted on Fig. 9. UE$_0$ is located close to the edge of its cell and is served by eNB$_0$ over $\mathbf{H}_0$. Additionally, UE$_0$ is in the vicinity of K interfering cells, where at least one UE per cell is served on the same physical resource as UE$_0$. Consequently, UE$_0$ experiences the transmissions from K eNBs as interference. We assume that the channel matrices from the interfering eNBs to their UEs $\mathbf{H}_k, k \in [1...K]$ change from the time instances n to $n+1$. For the sake of simplicity we further assume that each of the K UEs can react to this new downlink channel by selecting a new precoding matrix which is then applied at its serving eNB directly. Additionally, the selection is done by evaluating (22). Moreover, the channels $\mathbf{H}_k$ are correlated from time instance n to $n+1$ by a correlation coefficient $\tau_k \in [0...1]$.

B. Simulative Results

In the sequel we consider a setup with $K = 3$ interfering eNBs. Each interfering eNB transmits over $T_{1,2,3} = 4$ antennas with $L_1 = 1, L_2 = 2$ and $L_3 = 3$ spatial layers with the same transmit powers. UE$_0$ is assumed to be located close to its cell edge. For this setup the channel matrices $\mathbf{H}_k, \forall k \in [1...3]$ are assumed to be uncorrelated in time, i.e., $\tau_k = 0, \forall k \in [1...3]$. Figure 10 shows the trade-off between reduction of SINR

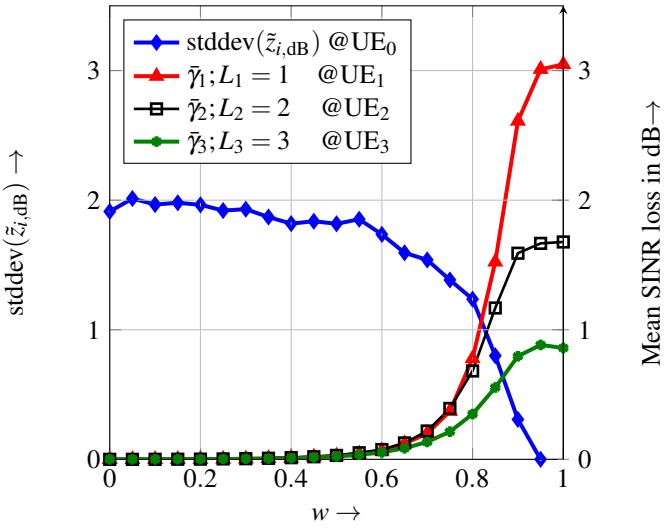

Fig. 10. Standard deviation of change in the SINR at UE$_0$ and corresponding SINR loss at different UEs in neighboring cells as a function of the weighting parameter w, $\tau_k = 0, \forall k \in [1...3]$ and $\xi = -3$ dB.

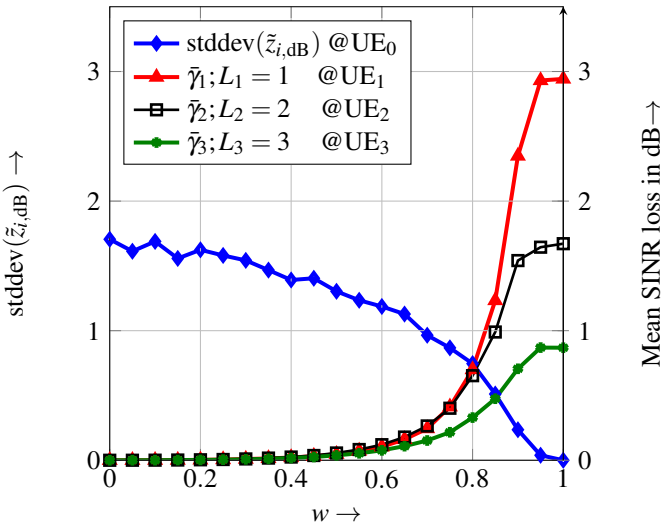

Fig. 11. Standard deviation of change in the SINR at UE$_0$ and corresponding SINR loss at different UEs in neighboring cells as a function of the weighting parameter w, $\tau_k = 0.7, \forall k \in [1...3]$ and $\xi = -3$ dB.

changes and SINR maximization. This figure clearly shows that SINR changes can be mitigated if UEs, scheduled at the same resource as UE$_0$ allow SINR losses, where the maximal SINR loss is higher at UEs that are served by a lower number of layers, e.g. $L_1 = 1$. Considering (23) it can be seen that the SINR cost function involves all layers at a UE. This results in an averaging over the SINR among the layers. Therefore it is more likely for single layer UEs to experience a high SINR loss. In this setup we consider $\xi = -3$ dB which corresponds to a scenario where the inter-cell interference power at UE$_0$ is twice the base-band noise power plus inter-layer interference power.

In contrast to the previous setup, Fig. 11 shows the standard deviation of the change in the SINR and the SINR loss trade-off for a scenario where the channels matrices $\mathbf{H}_k \forall k \in [1...3]$ are correlated from the time instances n to $n+1$ by $\tau_k = 0.7, \forall k \in [1...3]$. This investigation assumes that the downlink channels change slowly in time. In this case the UEs, UE$_k \forall k \in [1...3]$, do not have to change their precoding matrices every time instance and SINR variations in neighboring cells can be avoided by selecting the same precoding matrix again. Additionally, Fig. 11 clearly shows that SINR changes can already be decreased without suffering from visible SINR losses at UEs in other cells. The standard deviation of the change in the SINR can already be decreased by 1dB by allowing a negligible SINR loss at the UEs in a cell. This analysis shows that from a global point of view, each UE allows a slight SINR loss by setting the weighting w appropriately and thereby gains enhanced stability of the SINR. The purpose of this investigation is to show the potential gains by the application of such a weighting rule, the possible performance gains have to be investigated in extensive link-level simulations and field test, which are beyond the scope of this work.

VII. Conclusion

This paper provided a detailed analytical insight into low-rank inter-cell interference. We have shown that changes in the inter-cell interference are experienced at a UE if low-rank precoding matrices are reallocated in neighboring cells. Additionally, the severity of this change is strongly dependent on the combination of the currently allocated precoding matrix and the precoding matrix allocated at the next time instance. We derived the pdf of the change in the SINR that results from the change in the inter-cell interference. It could be shown that the standard deviation of this pdf is dependent on the ratio of inter-layer interference plus noise to inter-cell interference. Additionally, we proposed a novel UE specific precoding matrix selection rule that aims at jointly enhancing the SINR for a UE while reducing inter-cell interference and SINR changes in neighboring cells. It was shown that uncontrolled changes in the inter-cell interference can be reduced by approximately 1 dB by allowing negligible SINR losses at each UE.

Appendix A
Proof of Equation (9)

Without loss of generality, the ith diagonal element of $\mathbf{R}(n)$ can be expressed as $\sigma_k^2 \mathbf{g}^{(i)} \tilde{\mathbf{H}}_k \mathbf{B}_k(n) \mathbf{B}_k^H(n) \tilde{\mathbf{H}}_k^H \mathbf{g}^{(i)H}$. Furthermore, we write the Singular Value Decomposition of $\mathbf{g}^{(i)}$ in the following form

$$\mathrm{SVD}\left(\mathbf{g}^{(i)}\right) = [1]\,[0, \cdots, \sigma_i, 0, \cdots, 0_R]\,\mathbf{D}^H. \qquad (26)$$

The single singular value σ_i, which we write in the ith column, corresponds to the l_2-norm of the row-vector $\mathbf{g}^{(i)}$. With $\mathbf{D}^H \tilde{\mathbf{H}}_k \overset{d}{=} \tilde{\mathbf{H}}_k$ the vth diagonal element of $\mathbf{R}(n)$ can be expressed as

$$[\mathbf{R}(n)]_{v,v} = \sigma_k^2 \|\mathbf{g}^{(i)}\|_2^2 \tilde{\mathbf{h}}_k^{(i)} \mathbf{B}_k(n) \mathbf{B}_k^H(n) \tilde{\mathbf{h}}_k^{(i)H} \qquad (27)$$

Here $\overset{d}{=}$ denotes equality in distribution. Equation (27) can be reformulated as the sum of squared scalar products yielding,

$$[\mathbf{R}(n)]_{v,v} = \sigma_k^2 \|\mathbf{g}^{(i)}\|_2^2 \sum_{l=1}^{L_k} \left(\tilde{\mathbf{h}}_k^{(i)} \mathbf{b}_{k,(l)}(n)\right)^2 \qquad (28)$$

APPENDIX B
RATIO DISTRIBUTION OF THE BIVARIATE CHI-SQUARED DENSITY

To express the ratio distribution, the following short notation for z is introduced

$$z = \frac{u\,(n)}{u\,(n+1)} := \frac{u}{v}. \tag{29}$$

As mentioned before, $f_z\,(z)$ is independent of the layer index i, we therefore drop the layer index within this derivation. The distribution of $f_z\,(z)$ can now be found by solving

$$f_z(z) = \int_{v=0}^{\infty} v f_{u,v}\,(vz, v)\,dv. \tag{30}$$

The application of (30) on the definition of the joint bivariate chi-squared pdf taken from [15] leads to (31).

Further, the integral stated in (31) can be solved by application of the following substitutions

$$m = 2L_k \quad \nu = m + 2n \quad \mu = \frac{z+1}{2(1-\rho)}. \tag{32}$$

Subsequently, the integral in (31) can be solved by application of correspondence [16, 3.381.3] as

$$\int_{v=0}^{\infty} v^{\nu-1} e^{-\mu v} dv = \frac{1}{\mu^{\nu}}\Gamma\,(\nu)\,. \tag{33}$$

Substituting back into (31), replacing $m = 2L_k$ and $\rho = \rho_{k,u(n),(n+1)}$ yields (34)

The transformation of the pdf into dB scale is straightforward and yields

$$f_{z_{\mathrm{dB}}}\,(z_{\mathrm{dB}}) = 10^{\frac{z_{\mathrm{dB}}}{10}-1}\log(10) f_z\left(10^{\frac{z_{\mathrm{dB}}}{10}}\right). \tag{35}$$

APPENDIX C
RATIO DISTRIBUTION OF THE SHIFTED AND CORRELATED BIVARIATE CHI-SQUARED DISTRIBUTION

To derive the distribution of the change in the SINR $\tilde{z}_i$, we use the definition from (19) and perform the following substitution

$$z_i = \frac{\xi_i + u\,(n)}{\xi_i + u\,(n+1)} := \frac{\xi_i + u}{\xi_i + v}. \tag{36}$$

For the sake of simplicity, we drop the layer index i and perform the substitutions $\alpha = \xi_i + u$ and $\beta = \xi_i + v$ The joint pdf of numerator and denominator of (36) $f_{\alpha,\beta}(\alpha,\beta)$ can be found by the direct application of the introduced substitutions and we obtain

$$f_{\alpha,\beta}(\alpha,\beta) = f_{u,v}\,(\alpha - \xi_i, \beta - \xi_i)\,. \tag{37}$$

Where $f_{u,v}\,(\cdot,\cdot)$ is the bi-variate chi-squares pdf taken from [15]. The variable β has a support of $\beta \in [\xi_i, \infty]$ and the ratio distribution of $\tilde{z}_i$ can be found by solving [17] [18]

$$f_{\tilde{z}}(\tilde{z}) = \int_{\beta=\xi_i}^{\infty} \beta f_{u,v}\,(\beta\tilde{z} - \xi_i, \beta - \xi_i)\,d\beta, \quad \tilde{z} \geq 1. \tag{38}$$

Note, that $\tilde{z} \geq 1$ results from the fact that $f_{u,v}(u,v)$ is only defined for $u, v \geq 0$. The PDF of $\tilde{z}$ can be found by inserting the definition of the bivariate chi-square pdf from [15] into (38). The result is shown in (39)

The integral in (39) η can be split into two different parts with [16, 2.02.2] we have $\eta = \eta_1 + \eta_2$ with

$$\eta_1 = -\int_{\beta=\xi_i}^{\infty} \frac{(\beta-\xi_i)^{n+\frac{m}{2}}\, e^{-\frac{\xi_i}{\rho-1}+\frac{\beta(1+\tilde{z})}{2(\rho-1)}}\,(\beta\tilde{z}-\xi_i)^{n+\frac{m}{2}-1}}{\tilde{z}-1} d\beta \tag{40a}$$

$$\eta_2 = \int_{\beta=\xi_i}^{\infty} \frac{(\beta-\xi_i)^{n+\frac{m}{2}-1}\, e^{-\frac{\xi_i}{\rho-1}+\frac{\beta(1+\tilde{z})}{2(\rho-1)}}\,(\beta\tilde{z}-\xi_i)^{n+\frac{m}{2}}}{\tilde{z}-1} d\beta. \tag{40b}$$

Substituting in (40a),

$$m = 2L_k \quad v = \frac{2n+m}{2} \quad \alpha = \frac{1+\tilde{z}}{2(\rho-1)}$$
$$\phi = \frac{e^{-\frac{\xi_i}{\rho-1}+\alpha\xi_i}}{\tilde{z}-1} \quad \hat{\beta} = \beta - \xi_i \quad d = \xi_i - \frac{\xi_i}{\tilde{z}} \tag{41}$$

leads after fundamental algebraic manipulations to the simplified formulation

$$\eta_1 = -\phi\tilde{z}^{v-1}\int_{\hat{\beta}=0}^{\infty} \hat{\beta}^v((\hat{\beta}+d)^{v-1}e^{\alpha\hat{\beta}}d\hat{\beta} \tag{42}$$

If $v \in \mathbb{N}$ holds, (42) can be factorized by application of the binomial theorem [16, 1.111]. We obtain

$$\begin{aligned}\eta_1 &= -\phi\tilde{z}^{v-1}\int_{\hat{\beta}=0}^{\infty} \hat{\beta}^v \sum_{r=0}^{v-1}\binom{v-1}{r}\hat{\beta}^{v-1-r}d^r e^{\alpha\hat{\beta}}d\hat{\beta} \\ &= -\phi\tilde{z}^{v-1}\int_{\hat{\beta}=0}^{\infty} \sum_{r=0}^{v-1}\binom{v-1}{r}\hat{\beta}^{2v-1-r}d^r e^{\alpha\hat{\beta}}d\hat{\beta}\end{aligned} \tag{43}$$

We proceed by expanding (43) into a series. With [16, 2.323] we ca rewrite (43) according to.

$$\int P_v(\hat{\beta})e^{\alpha\hat{\beta}} = \sum_{p=0}^{v}(-1)^p\frac{P_v(\hat{\beta})^{(p)}}{\alpha^p}. \tag{44}$$

Where $P_v(\hat{\beta})^{(p)}$ denotes the pth derivative of the vth order polynomial in $\hat{\beta}$ with respect to $\hat{\beta}$. The integral (43) has to be evaluated for $\hat{\beta} = 0$ and $\hat{\beta} = \infty$. Since $\alpha < 0$ holds, (43) will converge to zero for $\hat{\beta} \to \infty$. Hence, the solution is determined from the point $\hat{\beta} = 0$ only. Substituting again,

$$P_{\eta_1} = \sum_{r=0}^{v-1}\binom{v-1}{r}\hat{\beta}^{2v-1-r}d^r e^{\alpha\hat{\beta}} \tag{45}$$

and differentiating (45) Q times results in (46).

Collecting the unequal zero summands in (46) results in

$$\frac{\partial^{v+j}P\eta_1}{\partial\hat{\beta}^{v+j}} = \binom{v-1}{v-j-1}(v+j)!d^{v-j-1}, \quad \text{for } 0 \leq j \leq v-1 \tag{47}$$

With the substitutions stated (41) the solution for (40a) can be given as

$$\eta_1 = \phi\tilde{z}^{v-1}\sum_{p=0}^{v-1}(-1)^{p+v}\binom{v-1}{v-p-1}(v+p)!d^{v-p-1}\frac{1}{\alpha^{p+v+1}} \tag{48}$$

The derivation of (40b) is analogously, with the substitutions stated in (41) the solution is

$$\eta_2 = -\phi\tilde{z}^{v}\sum_{p=-1}^{v-1}(-1)^{p+v}\binom{v}{v-p-1}(v+p)!d^{v-p-1}\frac{1}{\alpha^{p+v+1}}. \tag{49}$$

$$\begin{aligned} f_z(z) &= \int_{v=0}^{\infty} v f_{u,v}(vz, v)\, dv \\ &= \int_{v=0}^{\infty} \frac{z^{\frac{m-2}{2}} v^{m-1} e^{-\frac{vz+v}{2(1-\rho)}}}{2^m \sqrt{\pi}\Gamma\left(\frac{m}{2}\right)(1-\rho)^{\frac{m}{2}}} \sum_{n=0}^{\infty} \left[\frac{v\sqrt{\rho z}}{1-\rho}\right]^{2n} \frac{\Gamma\left(\frac{2n+1}{2}\right)}{(2n)!\Gamma\left(\frac{2n+m}{2}\right)} dv \\ &= \frac{1}{2^m \sqrt{\pi}\Gamma\left(\frac{m}{2}\right)(1-\rho)^{\frac{m}{2}}} \sum_{n=0}^{\infty} \left[\frac{\sqrt{\rho}}{1-\rho}\right]^{2n} \frac{\Gamma\left(\frac{2n+1}{2}\right)}{(2n)!\Gamma\left(\frac{2n+m}{2}\right)} \int_{v=0}^{\infty} z^{\frac{2n+m-2}{2}} v^{m-1+2n} e^{-\frac{vz+v}{2(1-\rho)}} dv \end{aligned} \tag{31}$$

$$f_z(z) = \frac{1}{2^{2L_k}\sqrt{\pi}\Gamma(L_k)(1-\rho)^{L_k}} \sum_{n=0}^{\infty} \left[\frac{\sqrt{\rho}}{1-\rho}\right]^{2n} \frac{\Gamma\left(\frac{2n+1}{2}\right)\Gamma(2n+2L_k) z^{n+L_k-1}}{(2n)!\Gamma(n+L_k)} \left[\frac{2(1-\rho)}{1+z}\right]^{2n+2L_k} \tag{34}$$

$$f_{\tilde{z}}(\tilde{z}) = \frac{\sum_{n=0}^{\infty}\left[\frac{\sqrt{\rho}}{1-\rho}\right]^{2n} \frac{\Gamma\left(\frac{2n+1}{2}\right)}{(2n)!\Gamma\left(\frac{2n+m}{2}\right)}}{2^m\sqrt{\pi}\Gamma\left(\frac{m}{2}\right)(1-\rho)^{\frac{m}{2}}} \underbrace{\int_{\beta=\xi_i}^{\infty} \beta\left(\beta\tilde{z}-\xi_i\right)^{\frac{2n+m-2}{2}} (\beta-\xi_i)^{\frac{2n+m-2}{2}} e^{-\frac{\beta\tilde{z}-\xi_i+\beta-\xi_i}{2(1-\rho)}} d\beta}_{\eta}. \tag{39}$$

$$\frac{\partial^Q P\eta_1}{\partial\hat{\beta}^Q} = \begin{cases} \sum_{r=0}^{v-1}\binom{v-1}{r}\hat{\beta}^{2v-1-r-Q}\prod_{z=1}^{Q}(2v-r-z)d^r, & \text{for } Q < v \\ \sum_{r=0}^{2v-Q-1}\binom{v-1}{r}\hat{\beta}^{2v-1-r-Q}\prod_{z=1}^{Q}(2v-r-z)d^r, & \text{for } v \le Q \le 2v-1 \end{cases} \tag{46}$$

Substituting back into (39) leads to the PDF for the SINR change on the ith layer given as (50).

with

$$\eta_1 = \phi\tilde{z}_i^{v-1}\sum_{p=0}^{v-1}(-1)^{p+v}\binom{v-1}{v-p-1}(v+p)!d^{v-p-1}\frac{1}{\alpha^{p+v+1}} \tag{51}$$

$$\eta_2 = -\phi\tilde{z}_i^{v}\sum_{p=-1}^{v-1}(-1)^{p+v}\binom{v}{v-p-1}(v+p)!d^{v-p-1}\frac{1}{\alpha^{p+v+1}}$$

and

$$\begin{aligned} d &= \xi_i - \frac{\xi_i}{\tilde{z}_i}, \qquad v = n + L_k \\ \phi &= \frac{e^{-\frac{\xi_i}{\rho-1}+\alpha\xi_i}}{\tilde{z}_i - 1}, \quad \alpha = \frac{1+\tilde{z}_i}{2(\rho-1)}, \quad \rho = \rho_{k,u(n),(n+1)}. \end{aligned} \tag{52}$$

The transformation of $f_{\tilde{z}_i}(\tilde{z}_i)$ into dB scale is straightforward and results in

$$f_{\tilde{z}_{i,\text{dB}}}(\tilde{z}_{i,\text{dB}}) = 10^{\frac{\tilde{z}_{i,\text{dB}}}{10}-1}\log(10) f_{\tilde{z}_i}\left(10^{\frac{\tilde{z}_{i,\text{dB}}}{10}}\right),\ \tilde{z}_{i,\text{dB}} \ge 0. \tag{53}$$

The variable $\tilde{z}_{i,\text{dB}}$ expresses the distribution of

$$\tilde{z}_{i,\text{dB}} = 10\log_{10}(\alpha) - 10\log_{10}(\beta), \tag{54}$$

which is the difference of two identically distributed variables with the same mean. Henceforth, the variable $\tilde{z}_{i,\text{dB}}$ has to have zero mean. Furthermore, for the change $\tilde{z}_{i,\text{dB}}$ holds

$$\tilde{z}_{i,\text{dB}} = \frac{\alpha}{\beta} \overset{d}{=} \frac{\beta}{\alpha}, \tag{55}$$

where $\overset{d}{=}$ denotes equality in distribution. This concludes that $f_{\tilde{z}_{i,\text{dB}}}(\tilde{z}_{i,\text{dB}})$ is symmetric around the mean value of 0 dB and the density function for negative values of $\tilde{z}_{i,\text{dB}}$ can be achieved as the positive density mirrored at zero yielding,

$$f_{\tilde{z}_{i,\text{dB}}}(\tilde{z}_{i,\text{dB}}) = \begin{cases} 10^{\frac{\tilde{z}_{i,\text{dB}}}{10}-1}\log(10) f_{\tilde{z}_i}\left(10^{\frac{\tilde{z}_{i,\text{dB}}}{10}}\right),\ \tilde{z}_{i,\text{dB}} \ge 0 \\ 10^{\frac{-\tilde{z}_{i,\text{dB}}}{10}-1}\log(10) f_{\tilde{z}_i}\left(10^{-\frac{\tilde{z}_{i,\text{dB}}}{10}}\right),\ \tilde{z}_{i,\text{dB}} \le 0. \end{cases} \tag{56}$$

APPENDIX D
DERIVATION OF THE CORRELATION MATRIX

The elements of $\mathbf{\Phi}_{x,y}$ denote the correlation of the post-equalizer inter-cell interference. We assume a linear equalizer and, therefore, it is sufficient to derive the correlation coefficient of the pre-equalizer inter-cell interference. To ease further analysis we write the the precoding matrix at the kth interfering eNB at the time instances n as $\mathbf{B}_{k,a}$ and time instance $n+1$ as $\mathbf{B}_{k,b}$, respectively.

Each correlation coefficient ρ_{x_i,y_j} can be found by solving

$$\rho_{x_i,y_j} = \frac{\mathrm{E}\big((x_i - \mathrm{E}(x_i))(y_j - \mathrm{E}(y_j))\big)}{\text{stdev}(x_i)\,\text{stdev}(y_j)}. \tag{57}$$

Since $\mathrm{E}(x_i) = \mathrm{E}(y_j) = \frac{\sigma_k^2}{L_k}$ and $\text{stdev}(x_i) = \text{stdev}(y_j) = \frac{\sigma_k^2}{L_k}$ holds, (57) simplifies to

$$\rho_{x_i,y_j} = \frac{\mathrm{E}(x_i y_j) - \mathrm{E}(x_i)\mathrm{E}(y_j)}{\text{stdev}(x_i)\,\text{stdev}(y_j)} = \frac{\mathrm{E}(x_i y_j) - \frac{\sigma_k^4}{L_k^2}}{\frac{\sigma_k^4}{L_k^2}} \tag{58}$$

Furthermore, $\mathrm{E}(x_i y_j)$ has to be written as

$$\begin{aligned} \mathrm{E}(x_i y_j) &= \sigma_k^4 \mathrm{E}\left(\tilde{\mathbf{h}}^H \mathbf{b}_{1,a,(l)}\mathbf{b}_{1,a,(l)}^H \tilde{\mathbf{h}}\tilde{\mathbf{h}}^H \mathbf{b}_{1,b,(l)}\mathbf{b}_{1,b,(l)}^H \tilde{\mathbf{h}}\right) \\ &= \sigma_k^4 \mathrm{E}\left(\mathrm{Tr}\left(\tilde{\mathbf{h}}\tilde{\mathbf{h}}^H \mathbf{b}_{1,a,(l)}\mathbf{b}_{1,a,(l)}^H \tilde{\mathbf{h}}\tilde{\mathbf{h}}^H \mathbf{b}_{1,b,(l)}\mathbf{b}_{1,b,(l)}^H\right)\right) \end{aligned} \tag{59}$$

$$f_{\tilde{z}_i}(\tilde{z}_i) = \frac{1}{2^{2L_k}\sqrt{\pi}\Gamma(L_k)(1-\rho)^{L_k}} \sum_{n=0}^{\infty} \left[\frac{\sqrt{\rho}}{1-\rho}\right]^{2n} \frac{\Gamma\left(\frac{2n+1}{2}\right)}{(2n)!\Gamma(L_k+n)} \left[\eta_1+\eta_2\right], \ \tilde{z}_i \geq 1 \quad (50)$$

We denote the outer product $\mathbf{W} = \tilde{\mathbf{h}}\tilde{\mathbf{h}}^H$ as a complex Wishart matrix with covariance Matrix $\mathbf{\Sigma} = \mathbf{I}$. Utilizing known correspondences for the Wishart matrix taken from [19] yields in combination with (59) to

$$\mathrm{E}(x_u y_v) = \sigma_k^4 \mathrm{Tr}\left(\mathrm{E}\left(\mathbf{W}\mathbf{b}_{1,a,(l)}\mathbf{b}_{1,a,(l)}^H\mathbf{W}\right)\mathbf{b}_{1,b,(l)}\mathbf{b}_{1,b,(l)}^H\right), \quad (60)$$

where

$$\begin{aligned}\mathrm{E}\left(\mathbf{W}\mathbf{b}_{1,a,(l)}\mathbf{b}_{1,a,(l)}^H\mathbf{W}\right) &= \\ \mathbf{b}_{1,a,(l)}\mathbf{b}_{1,a,(l)}^H + \mathrm{Tr}\left(\mathbf{b}_{1,a,(l)}\mathbf{b}_{1,a,(l)}^H\right) &\\ = \mathbf{b}_{1,a,(l)}\mathbf{b}_{1,a,(l)}^H + \frac{1}{L_k} &\end{aligned} \quad (61)$$

Substituting (61) back into (60) leads to

$$\begin{aligned}&\mathrm{E}(x_i y_j) = \\ &\sigma_k^4 \mathrm{Tr}\left(\mathbf{b}_{1,a,(l)}\mathbf{b}_{1,a,(l)}^H\mathbf{b}_{1,b,(l)}\mathbf{b}_{1,b,(l)}^H\right) + \frac{\sigma_k^4}{L_k}\mathrm{Tr}\left(\mathbf{b}_{1,b,(l)}\mathbf{b}_{1,b,(l)}^H\right) \\ &= \sigma_k^4 \mathrm{Tr}\left(\mathbf{b}_{1,a,(l)}\mathbf{b}_{1,a,(l)}^H\mathbf{b}_{1,b,(l)}\mathbf{b}_{1,b,(l)}^H\right) + \frac{\sigma_k^4}{L_k^2}\end{aligned} \quad (62)$$

Substituting (62) back into (58) leads to

$$\rho_{x_i,y_j} = \mathrm{Tr}\left(\mathbf{b}_{1,a,(l)}\mathbf{b}_{1,a,(l)}^H\mathbf{b}_{1,b,(l)}\mathbf{b}_{1,b,(l)}^H\right)L_k^2, \quad (63)$$

which equals (10).

1) Proof of the Approximation stated in Equation (14)*:* (9) can be interpreted as

$$z = \frac{\sum_{l=1}^{L_k} x_i}{\sum_{l=1}^{L_k} y_i} := \frac{u}{v}, \quad (64)$$

where u and v obey to two chi-square distributions with $2L_k$ degree of freedom. A reasonable step is to calculate the correlation coefficient between u and v. The derivation can be obtained by substituting

$$\begin{aligned}\mathbf{b}_{1,a,(l)} \Rightarrow \mathbf{B}_{1,a} \quad \mathbf{b}_{1,b,(l)} \Rightarrow \mathbf{B}_{1,b}& \\ \mathrm{E}(x_i) \Rightarrow \mathrm{E}(u) = \frac{\sigma_k^2}{2L_k} \quad \mathrm{E}(y_j) \Rightarrow \mathrm{E}(v) = \frac{\sigma_k^2}{2L_k}& \\ \mathrm{stdev}(x_i) \Rightarrow \mathrm{stdev}(u) = \frac{\sigma_k^2}{\sqrt{L_k}}& \\ \mathrm{stdev}(y_j) \Rightarrow \mathrm{stdev}(v) = \frac{\sigma_k^2}{\sqrt{L_k}}&\end{aligned}$$

into the derivation of (63). Noting that for any precoding matrix $\mathrm{Tr}\left(\mathbf{B}\mathbf{B}^H\right) = 1$ holds, leads to (14).

REFERENCES

[1] I. Telatar, "Capacity of Multi-antenna Gaussian Channels," *European Transactions on Telecommunications*, vol. 10, no. 6, pp. 585–595, November/December 1999.

[2] A. Scaglione, P. Stoica, S. Barbarossa, G. Giannakis, , and H. Sampath, "Optimal designs for space-time linear precoders and decoders," *IEEE Transactions on Signal Processing*, vol. 50, no. 5, pp. 1051 –1064, May 2002.

[3] D. Love and R. Heath, "Limited feedback unitary precoding for spatial multiplexing systems," *IEEE Transactions on Information Theory*, vol. 51, no. 8, pp. 2967 – 2976, August 2005.

[4] S. Schwarz, M. Wrulich, and M. Rupp, "Mutual Information based Calculation of the Precoding Matrix Indicator for 3GPP UMTS/LTE," in *International ITG Workshop on Smart Antennas (WSA)*, Bremen, Germany, February 2010, pp. 52 –58.

[5] "Physical Channels and Modulation (Release 8)," Technical Specification Group Radio Access Network 3GPP TS 36.211 V8.8.0, Tech. Rep., 2009.

[6] M. Rumney, *LTE and the Evolution to 4G wireless: Design and Measurement Challenges*, reprinted ed. Chichester, UK: Wiley and Sons, 2009.

[7] Z. Wang, X. Zhang, G. Wei, and Y. Wang, "A novel Inter-Cell Interference mitigation Scheme for Downlink of LTE-Advanced Systems," in *3rd IEEE International Conference on Broadband Network and Multimedia Technology (IC-BNMT)*, Beijing, China, October 2010, pp. 593 –597.

[8] A. Simonsson, "Frequency Reuse and Intercell Interference Co-Ordination In E-UTRA," in *IEEE Vehicular Technology Conference, (VTC)*, Dublin, Ireland, April 2007, pp. 3091 –3095.

[9] L. Falconetti and C. Hoymann, "Codebook based Inter-Cell Interference Coordination for LTE," in *IEEE 21st International Symposium on Personal Indoor and Mobile Radio Communications (PIMRC)*, Istanbul, Turkey, September 2010, pp. 1769 –1774.

[10] J. Giese and M. Amin, "Performance Upper Bounds for coordinated Beam selection in LTE-Advanced," in *International ITG Workshop on Smart Antennas (WSA)*, Bremen, Germany, February 2010, pp. 280 – 285.

[11] D. Lee, H. Seo, B. Clerckx, E. Hardouin, D. Mazzarese, S. Nagata, and K. Sayana, "Coordinated multipoint transmission and reception in lte-advanced: deployment scenarios and operational challenges," *Communications Magazine, IEEE*, vol. 50, no. 2, pp. 148 – 155, February 2012.

[12] F. Monsees, C. Bockelmann, M. Petermann, A. Dekorsy, S. Brueck, and J. Giese, "On the SINR Distribution of Codebook-Based Precoding in LTE in Case of Inter-Cell Interference," in *8th International Symposium on Wireless Communication Systems (ISWCS 11)*, Aachen, Germany, Nov 2011.

[13] D. Tse and P. Viswanath, *Fundamentals of Wireless Communication*. Cambrige University Press, 2005.

[14] M. Hagedorn, P. Smith, P. Bones, R. Millane, and D. Pairman, "A trivariate chi-squared distribution derived from the complex wishart distribution," *Journal of Multivariate Analysis*, vol. 97, no. 3, pp. 655 – 674, 2006.

[15] A. Joarder, "Moments of the Product and Ratio of two Correlated Chi-Square variables," *Statistical Papers*, vol. 50, pp. 581–592, 2009.

[16] I. S. Gradshteyn and I. M. Ryshik, *Table of Integrals, Series, and Products*, 6th ed. London: Academic Press, 2000.

[17] A. Papoulis and S. U. Pillai, *Probability, Random Variables, and Stochastic Processes*, 4th ed. New York: Mc Graw Hill, 2002.

[18] N. Johnson and S. Kotz, *Distributions in Statistics Continuous Multivariate Distributions*. New York: Wiley, 1972.

[19] J. A. Tague and C. I. Caldwell, "Expectations of useful complex Wishart forms," *Multidimensional Systems and Signal Processing*, vol. 5, pp. 263–279, 1994.

Fabian Monsees received his B.Sc. degree in Electrical Engineering from the University of Applied Sciences Bremen in 2009. He received his M.Sc. degree in Communication and Information Technology from the University of Bremen in 2011. He is currently working towards his PhD degree at the Institute for Telecommunications and High-Frequency Techniques. Special research interests are Compressed Sensing, Multi-User Detection, Sparse Communication Models, Machine-to-Machine Communication and Pre-coding.

Dr.-Ing. Carsten Bockelmannn received his Dipl.-Ing. degree in electrical engineering in 2006 and his PhD degree 2012 both in electrical engineering and from the University of Bremen, Germany. Since 2012 he is working as a post doctoral researcher at the University of Bremen coordinating research activities regarding the application of compressive sensing/sampling to communication problems. His current research interests include compressive sensing and its application in communications contexts, as well as channel coding and transceiver design.

Dr.-Ing. Mark Petermann received the Dipl.-Ing. degree in electrical engineering from the University of Bremen, Germany, in 2005. From 2005 to 2012 he was with the Department of Communications Engineering at the University of Bremen, where he received the Dr.-Ing. degree in 2012. Currently, he is with the ATLAS ELEKTRONIK GmbH. His main fields of interest are multi-user MIMO communications, image and correlation processing.

Prof. Armin Dekorsy holds the chair of the Department of Communications Engineering, University of Bremen, since April 2010. He received his Dipl.-Ing. (FH) (B.Sc.) degree from Fachhochschule Konstanz, Germany; Dipl.-Ing. (M.Sc.) degree from University of Paderborn, Germany; PhD degree from the University of Bremen, Germany, all in communications engineering. From 2000 to 2007 he worked as research engineer at Deutsche Telekom AG and as Distinguished Member of Technical Staff (DMTS) at Bell Labs Europe, Lucent Technologies. In 2007 he joined Qualcomm GmbH as European Research Coordinator conducting Qualcomms' internal and external European research projects like ARTIST4G, BeFemto, and WINNER+. His current research interests include resource management, transceiver design and digital signal processing for wireless communications systems in health care, automation and mobile communications. Prof. Dekorsy is member of ITG expert committee "Information and System Theory", VDE and IEEE communications and signal processing society.

Dr-Ing. Stefan Brueck studied mathematics and electrical engineering at University of Technology Darmstadt, Germany and Trinity College Dublin, Ireland. He received his Dipl.-Math. and Dr.-Ing. degrees in 1994 and 1999, respectively. From 1999 to 2008 he was working for Lucent Technologies and Alcatel-Lucent in Bell Labs and UMTS Systems Engineering, where he was responsible for the MAC layer design of the HSPA base station. In May 2008 he joined Qualcomm Research and was active in several research projects and standardization activities related to LTE and LTE-Advanced. Currently, his research focuses on physical layer design for high data rate transmission over coaxial cable.